INT. J. REMOTE SENSING, 2001, VOL. 22, NO. 5, 807–817

Analysing potential cliff erosivity from ERS SAR satellite imagery

N. MANSPEIZER

Graduate School of Geography, Clark University, 950 Main Street, Worcester, MA 01610, USA; e-mail: nmanspeizer@clarku.edu

A. KARNIELI

The Remote Sensing Laboratory, J. Blaustein Institute for Desert Research, Ben Gurion University, Sede Boqer Campus 84990, Israel

Y. ARKIN

Geological Survey of Israel, 30 Malkhe Israel St., Jerusalem 95501, Israel

and J. CHOROWICZ

LGGST, Case 129, Paris 6 University, 4 Place Jussieu, 75252 Paris cedex 05, France

(Received 14 July 1998; in final form 1 September 1999)

Abstract. This paper demonstrates a method to elucidate potential erosivity (PE) of cliff strata that fall within the radar shadow of European Remote Sensing (ERS) Synthetic Aperture Radar (SAR) imagery. ERS-1 imagery of cliff faces in Israel's Negev Desert that faced 'away' from the satellite look direction contained alternating grey/black stripes that corresponded to the sedimentological units that make up the cliffs. High return values or digital numbers (DN) relate to gently sloping surfaces with softer lithologies that yield higher rates of weathering. Conversely, lower return values (DN) represent steeper surfaces with harder lithologies that yield a slower rate of weathering. Backscatter and Z-score values were extracted from the image to derive an index of PE for strata at the feature and sub-feature level. This method may be used to determine relative erosivity of cliff strata, compliment existing geological mapping techniques and refine topographical representation of cliff faces in existing digital elevation models (DEMs).

1. Introduction

Synthetic Aperture Radar (SAR) satellite systems actively illuminate the terrain with pulses of long-wave electromagnetic energy and detect the strength of the returning pulse. The surface roughness, slope and orientation of the topography in the look direction of the radar system determines the intensity of the returning pulse, or its back-scatter. Cliffs and ridges that face away from the radar look direction reflect little or no energy, since the transmitted pulses do not reach these areas. These 'radar shadows' have traditionally been thought to contain little information and have, therefore, been the subject of limited research. This paper presents a method of analysing the reduced backscatter values within the shadow of a 'forward-facing' cliff that is oriented away from the look direction of the radar system.

International Journal of Remote Sensing
ISSN 0143-1161 print/ISSN 1366-5901 online © 2001 Taylor & Francis Ltd
http://www.tandf.co.uk/journals

In arid regions, the dominant forces of weathering are mechanical processes, controlled by the movement of water and wind. The potential erosivity (PE) and subsequent topography or cliff slope is a result of the lithostratigraphy of the strata that comprise the cliff face. Strata with softer lithologies yield higher rates of erosion and form gently sloping surfaces, while steeper surfaces or cliffs are formed by strata with harder lithologies that yield a slower rate of erosion. Cliffs comprised of stratified sedimentary rock units in arid regions often display a stair-stepped morphology typical of mesas, due to the subsequent resistance of alternating rock strata. As figure 1 indicates, exposed formations with the most-resistant beds, such as dolomite and limestone in arid regions, form the most conspicuous cliff faces. Exposed formations with relatively soft lithologies, such as friable sandstone and argillaceous limestone in arid regions, form talus slopes.

The incidence angle of SAR satellite systems, such as the 23° at mid-swath for the European Remote Sensing system ERS-1, highlights these erosion patterns by receiving lower return values for cliff faces and higher return values for talus slopes. This is only true when the look direction of the SAR system is the same as the 'look direction' of the cliff face, and the SAR satellite is located 'behind' the cliff (figure 1). According to Berlin et al. (1982), backscatter intensity along these forward-facing cliffs is largely due to changes in ground slope between more-resistant and less-resistant strata, rather than surface roughness. Therefore, one would expect to find the beds with the most-resistant rock to display lower backscatter values, and beds with less-resistant rock, or talus slopes, to display higher backscatter values.

The aim of the present study was to identify lithologies in a cliff face and compare these lithologies to their corresponding backscatter values in order to quantify the PE of each stratum based on its backscatter value. This method may be used to determine relative erosivity of cliff strata in areas where fieldwork possibilities are

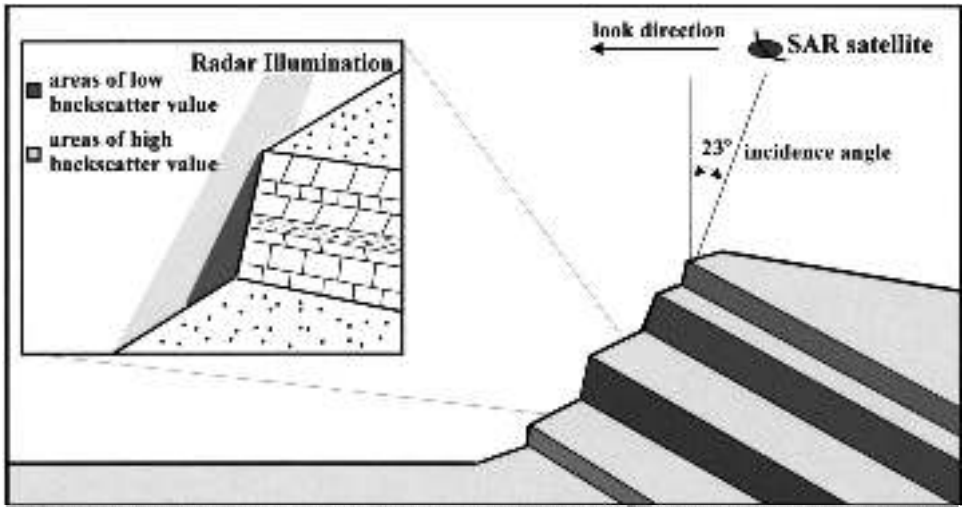

Figure 1. Illumination of a cliff face by Synthetic Aperture Radar (SAR) as seen from the side when the cliff is oriented 'away' from the satellite look direction. The alternating beds of resistant to less-resistant strata are dipping steeply away from the cliff face, and the satellite is situated 'behind' the cliff. The resulting radar backscatter appear as alternating stripes, where steep slopes have lower backscatter values than talus slopes (see figure 3).

limited, as well as refining the topographical representation of cliff faces in existing digital elevation models (DEMs).

2. Study site

The study was conducted in the Makhtesh Hakatan (the 'Little Crater'), which is an erosional cirque in the north-eastern Negev Desert in Israel. The crater, shown in three-dimensional orthographic display in figure 2, is not actually a crater, but rather an eroded bowl or cirque of a breached anticline. As anticlinal crests are subjected to tectonic stress (much like a multi-layered cake pushed up from the bottom), cracks form in the top of the dome. These cracks eventually deepen and widen by precipitation and wind to form a round cavity with perpendicular walls. While surface water flow erodes the cirque bottom, the walls retain their vertical face. As erosion of the cirque bottom increases and the cliff wall is exposed, the tilted strata of the ancient anticline are revealed (Orni and Efrat 1976).

Figure 3 shows the 16-bit ERS-1 radar image of the Little Crater with a spatial resolution of 25 m. The look direction of the radar system is towards the west, and the image reveals banding along the eastern wall of the crater. This eastern cliff face is also oriented towards the west and away from the look direction of the satellite. Note that this same banding does not appear along the western wall. In this case, high return values are shown here in light grey and lower return values are shown in the darker-grey/black pixels. Fieldwork was carried out in the summer of 1997 to determine the origin of these distinctive banding patterns. The fieldwork concentrated on the north-east wall of the crater, where the banding was most prominent and where more discrete bands could be identified in the radar image.

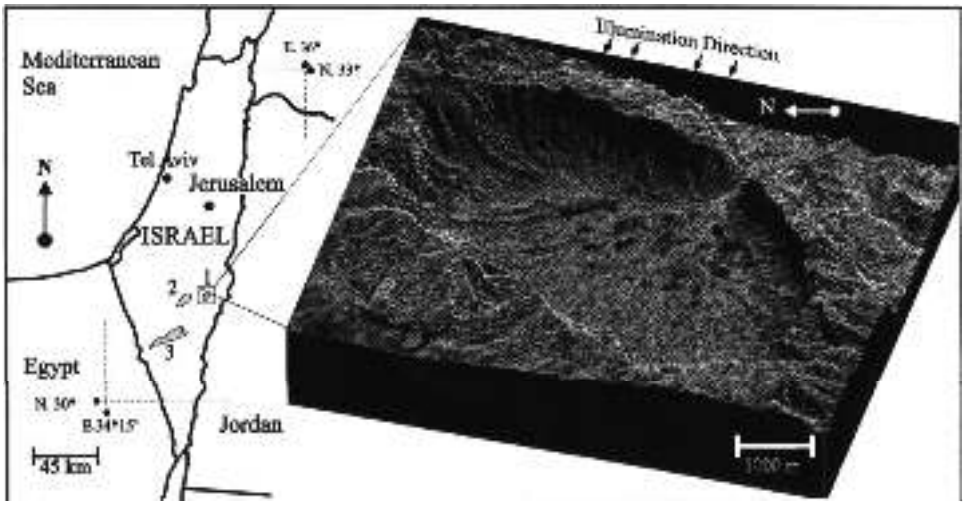

Figure 2. Study site in the northern Negev Desert in Israel. Makhtesh Hakatan (the 'Little Crater') is shown (1) in three-dimensional orthographic display of a true colour Landsat Thematic Mapper composite draped over a digital terrain model (DTM). The orthographic image is looking towards the north-east and has been rotated 90° counter-clockwise of north to reveal the north-east wall of the crater. Similiar banding patterns were also found along the eastern walls of SAR imagery of the 'Big Crater' (2) and 'Ramon Crater' (3) in the Negev Desert.

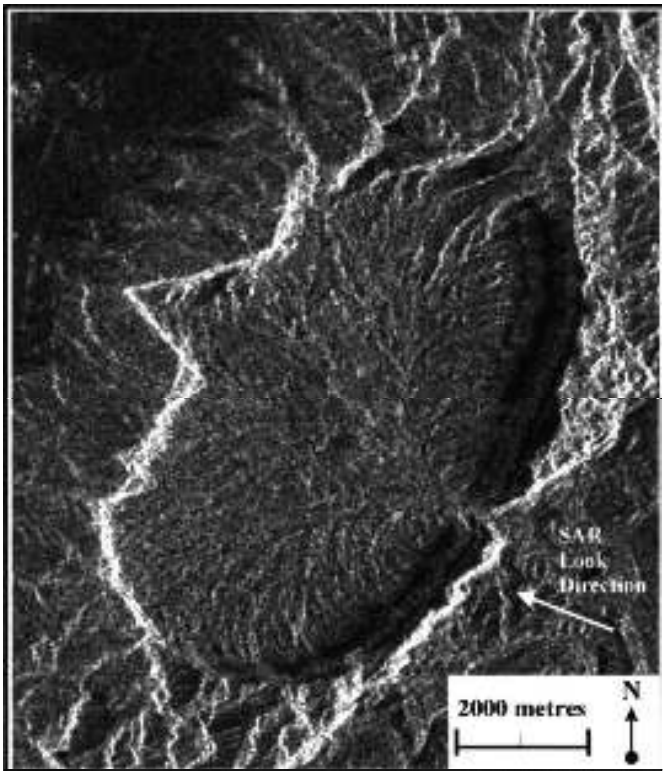

Figure 3. ERS-1 image of the Little Crater. Note the banding patterns along the eastern wall.

3. Data analysis and results

The erosional patterns discussed above (e.g. alternating cliff and talus slopes) were identified in the field by correlating geological maps (Hirsch 1996) and cross-sections (Arkin and Braun 1965) to the north-east cliff wall (figure 4). The beds that comprise the cliff wall are approximately 360 m high, striking N–S and dipping roughly 55°. At the cliff base, the coloured sands of the Hatira Formation are exposed. The Hatira Formation is composed of Nubian sandstones and clays of Lower Cretaceous age and form a talus slope. A cliff face within the Hatira Formation is formed by a marine ingression comprised of limestone and marl. The Hevyon Formation is composed of limestone and dolomite and forms a massive, nearly vertical cliff. The En Yorqeam Formation comprises five identifiable sub-units: the first and third sub-units are argillaceous limestone and marl that form talus slopes; the second and fourth sub-units are both silicified limestone that form two small cliff faces; and the fifth sub-unit is a talus slope consisting of limestone, argillaceous limestone and clay. The Zafit Formation has a characteristic red-brown colour, and is composed of massively bedded limestones and dolomites that form a distinct cliff. There are two distinct sub-units within the Avnon Formation: the first sub-unit consists of marls and limestones that form a talus slope; the second sub-unit consists of a hard massive limestone and dolomite complex that forms a conspicuous cliff (figure 4).

The cliff strata identified in the field were then compared visually with the ERS-1

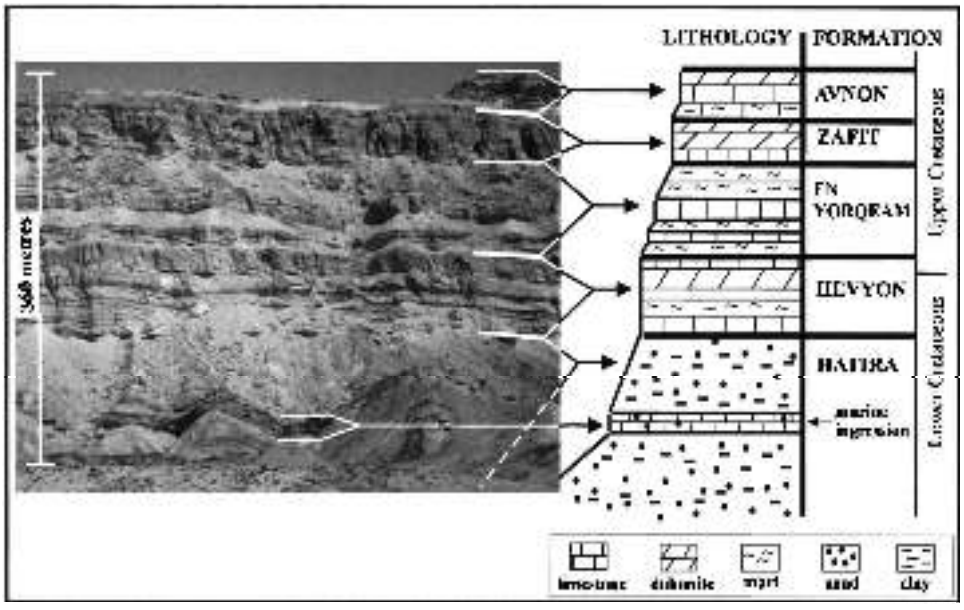

Figure 4. Lithostratigraphy of the north-east cliff face of the Little Crater. Sources: Arkin and Braun (1965) and Hirsch (1996).

image to correlate the strata with the banding patterns. The alternating grey/black stripes within the image were identified as corresponding to the sedimentological units that make up the cliff. Both formation and sub-formation level features were discernible with the 25 m spatial resolution of the ERS-1 image (figure 5).

Training sets were developed for each formation and sub-formation in order to derive a relative PE index (PEI) for each feature based on their backscatter (figure 5). The training sets were developed based on interpretation of the field geology and radar image and according to accepted standards for training-set development (e.g. consideration of pixel numbers and homogeneity). Statistics for each training set were then extracted from the raw ERS-1 image using IDRISI, a raster Geographical Information System (GIS) software package, to determine the mean, minimum, maximum and sample standard deviation from the mean for each training set. In order to derive a meaningful PEI, and compensate for the non-normal distribution found in the raw ERS-1 image, Z-score values were extracted for each training set. The Z-score image was calculated as the difference between the values of the log normal transform of each pixel ($\log(X)$) and the mean value image (μ) divided by the standard deviation image (σ):

$$Z\text{-score} = (\log(X) - \mu)/\sigma \tag{1}$$

While the relationships between the training sets are similar to the raw image, the differentiation is more apparent and statistically meaningful (figure 6 and table 1).

The PEI was then derived by standardizing the mean Z-score values of each training set in relation to the maximum and minimum values for all of the training sets:

$$\text{PEI} = 10 - ((\max_{Z\text{-score}} - \mu_{Z\text{-score}})/(\max_{Z\text{-score}} - \min_{Z\text{-score}})) \tag{2}$$

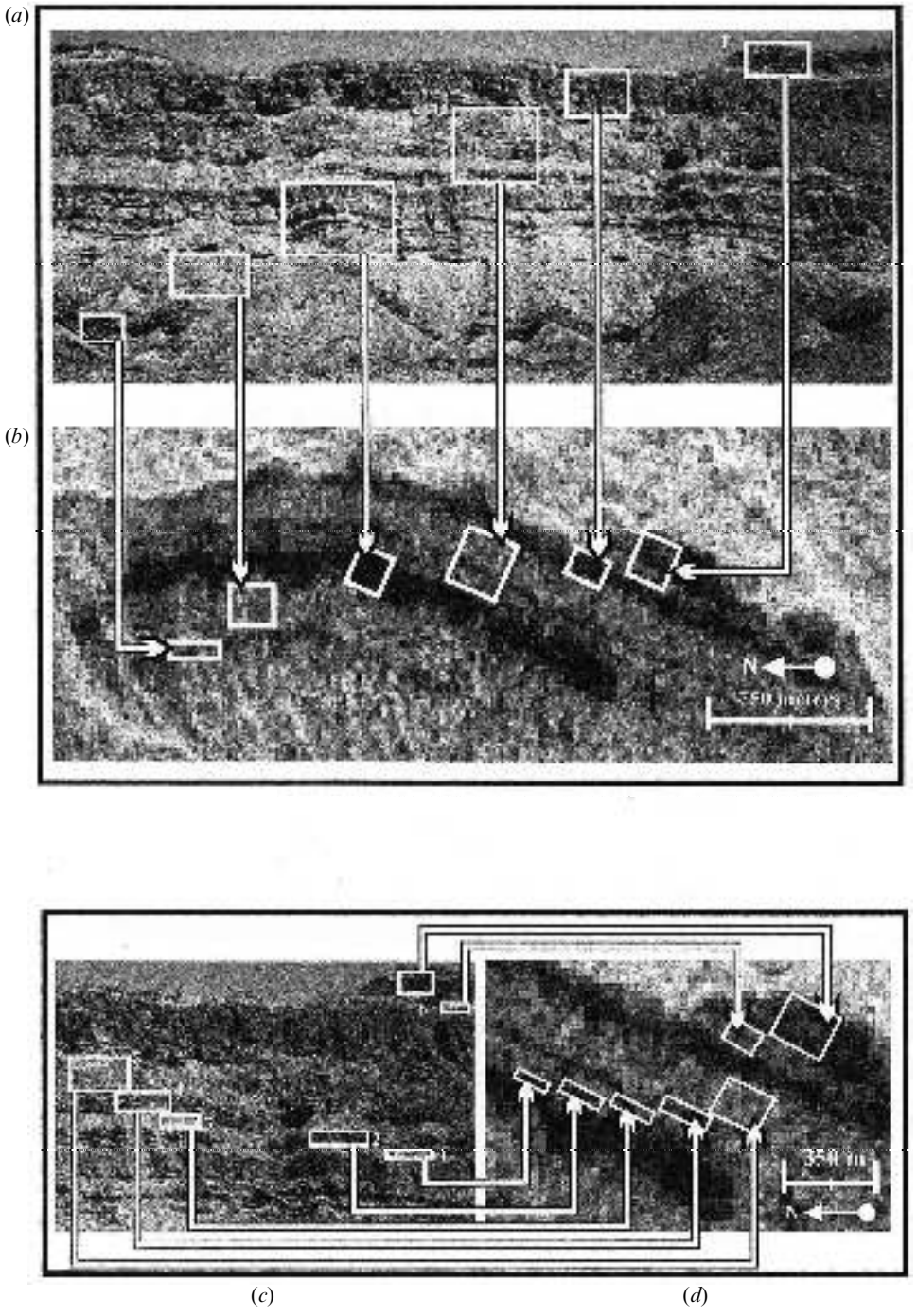

Figure 5. Identification of formation level features in photo (a) and ERS-1 image (b) of the north-east crater wall (A, marine ingression; B, Hatira; C, Hevyon; D, En Yorqeam; E, Zafit; F, Avnon). Identification of sub-formation level features in enlargements of photo (c) and ERS-1 image (d) of the north-east cliff wall (1–5, En Yorqeam sub-units A–E; 6–7, Avnon sub-units A–B).

In this index, higher values have relatively more potential for erosivity than lower values. In other words, a PE value of 1 indicates a harder lithology resistant to erosion, while a PE value of 10 indicates a softer and more easily eroded lithology (figure 6 and table 1).

4. Discussion

The training-set statistics from the ERS-1 image indicate that those formations and sub-units with harder lithologies that are more resistant to erosion and appear as cliff faces have lower backscatter values than those formations with softer lithologies that form talus slopes (table 1). For example, the Hevyon Formation, composed of well-bedded limestone and dolomite, has an average backscatter of 82.33, while the En Yorqeam Formation, composed of interbedded argillaceous limestone and marl, has an average backscatter of 187.24. Features were also successfully differentiated at the sub-formation level. For example, sub-unit A of the Avnon Formation, composed of micro-crystalline limestone and marl, has an average backscatter of 174.0, while sub-unit B, composed of limestone and dolomitic limestone, has an average backscatter of 95.42 (figure 6 and table 1).

There are two significant findings that are conveyed in these results. Firstly, lithology is a clear determinant of backscatter value. Formations and sub-units of parent material that produce talus slopes, such as friable sandstone or marl, are more susceptible to erosion and yield a higher backscatter value. The Hatira Formation, composed of friable sandstone and clay and yielding a PE of 6.44, is a good example. Conversely, formations and sub-units with more consolidated parent material, such as dolomites and well-bedded limestone, are less susceptible to erosion and produce a cliff face that yields a higher backscatter value. For example, the Hevyon Formation, composed of well-bedded limestone and dolomite, has a PE of 3.06.

Secondly, the 25 m spatial resolution of this imagery allowed us to differentiate features at both formation and sub-formation levels. While the En Yorqeam and Avnon formations have an overall PE value at the formation level, they can be separated into sub-units to give us a more detailed understanding of potential cliff erosion (table 1). Some of the backscatter values along the edges of training sets are the result of mixed pixels due to detritus that has eroded from parent material higher in the cliff face. This problem, and improved differentiation at the sub-formation level, may be alleviated with the use of SAR sensors with a finer spatial resolution than the 25 m used here.

5. Conclusions

This paper presents a method of developing a PEI using radar shadow bands for a forward-facing cliff, based on backscatter value in a SAR satellite image. This was accomplished by identifying the lithology in the cliff face, comparing the cliff strata lithologies to their corresponding backscatter values and quantifying the PE of each stratum based on this value (figure 7).

Backscatter intensity along these forward-facing cliffs is largely due to changes in ground slope between more-resistant and less-resistant strata. Beds composed of more-resistant rock display lower backscatter values, whereas beds of less-resistant rock or talus slopes display higher backscatter values.

This method may be used as an aid in current geologic mapping strategies to identify shadow hidden features that are lithostratigraphically significant at the

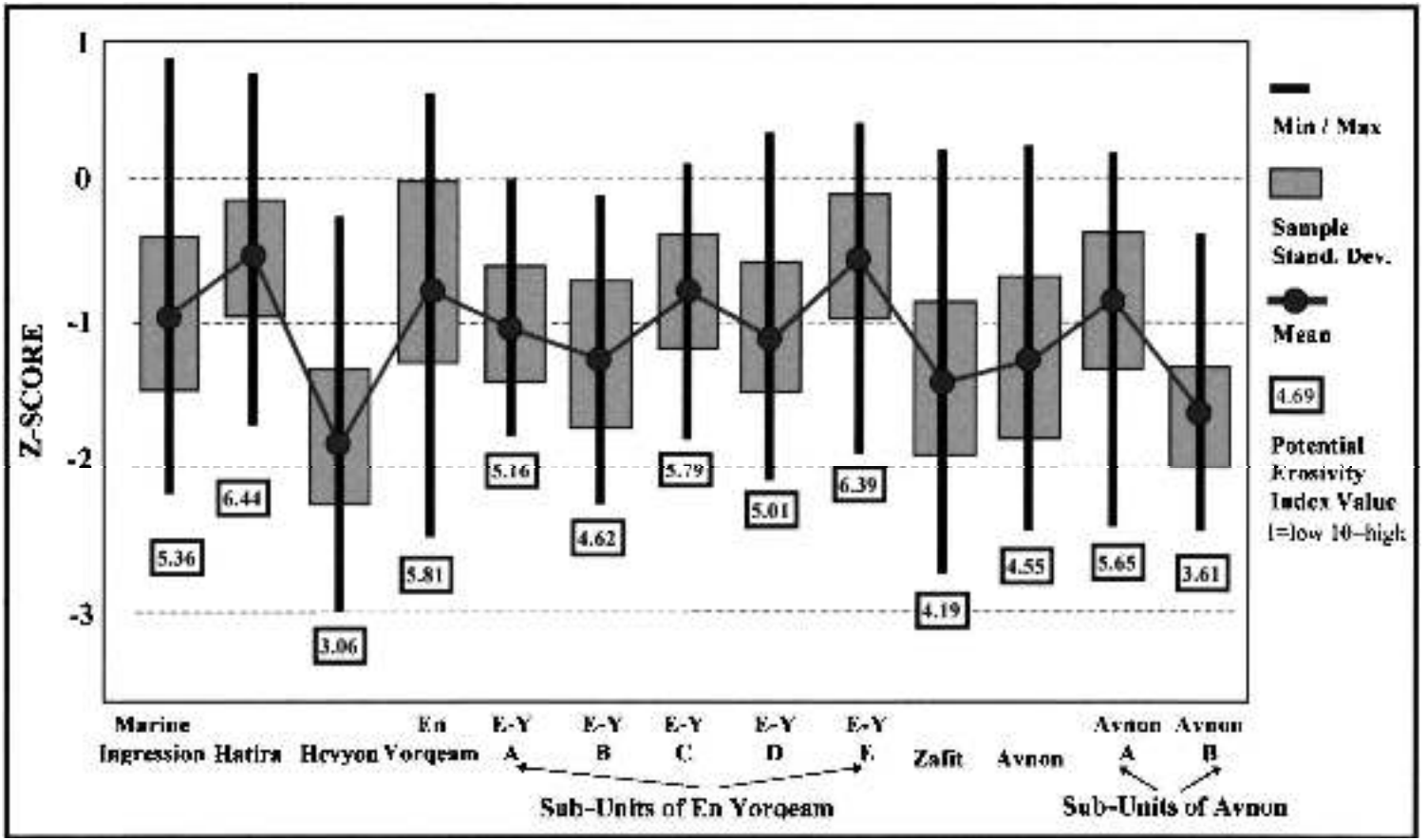

Figure 6. Z-score and potential-erosivity statistics for training sets derived from log-transformed image for formations and sub-formation level units.

Table 1. Lithology and extracted statistics for formation and sub-formation training sets. Lithology index: **[**10 − ((max$_{Z\text{-score}}$ − mean$_{Z\text{-score}}$)/(max$_{Z\text{-score}}$ − min$_{Z\text{-score}}$))**]**. *Z*-score: **[**(log-normal transfer image − mean value image)/standard deviation image**]**.

Formation/training-set	Lithology*	Mean DN†	Max./min. DN†	Sample standard deviation†	Mean *Z*-score‡	Potential erosivity (1 = low, 10 = high)	Potential erosivity standard deviation
Marine ingression	Limestone to marl, sand	163.76	608/57	67.02	− 0.945	**5.36**	0.51
Hatira	Friable sandstone, clay	220.91	548/89	69.83	− 0.53	**6.44**	0.98
Hevyon	Well-bedded limestone dolomite and marl	82.33	264/31	33.26	− 1.83	**3.06**	1.02
En Yorqeam	Argillaceous limestone and marl	187.24	514/47	67.63	− 0.77	**5.81**	0.65
A	Argillaceous limestone and marl	151.87	310/80	51.33	− 1.02	**5.16**	0.52
B	Silicified limestone	130.67	283/56	48.57	− 1.23	**4.62**	0.59
C	Argillaceous limestone and marl	181.41	343/78	52.36	− 0.78	**5.79**	0.56
D	Silicified limestone	147.87	393/63	59.41	− 1.08	**5.01**	0.54
E	Argillaceous limestone, interbedded clay	216.96	431/74	62.34	− 0.55	**6.39**	0.79
Zafit	Massive bedded limestone and dolomite	117	373/39	48.65	− 1.4	**4.19**	0.71
Avnon	Limestone, dolomite underlain by limestone, marl	135.56	379/48	61.05	− 1.22	**4.55**	0.64
A	Micro-crystalline limestone, marl	174	367/49	53.07	− 0.84	**5.65**	0.51
B	Limestone and dolomitic limestone	95.42	231/48	32.3	− 1.62	**3.61**	0.87

*Source: Arkin and Braun (1965) and Hirsch (1996).
†Raw ERS-1 image. Digital Number (DN).
‡Log normal transform image.

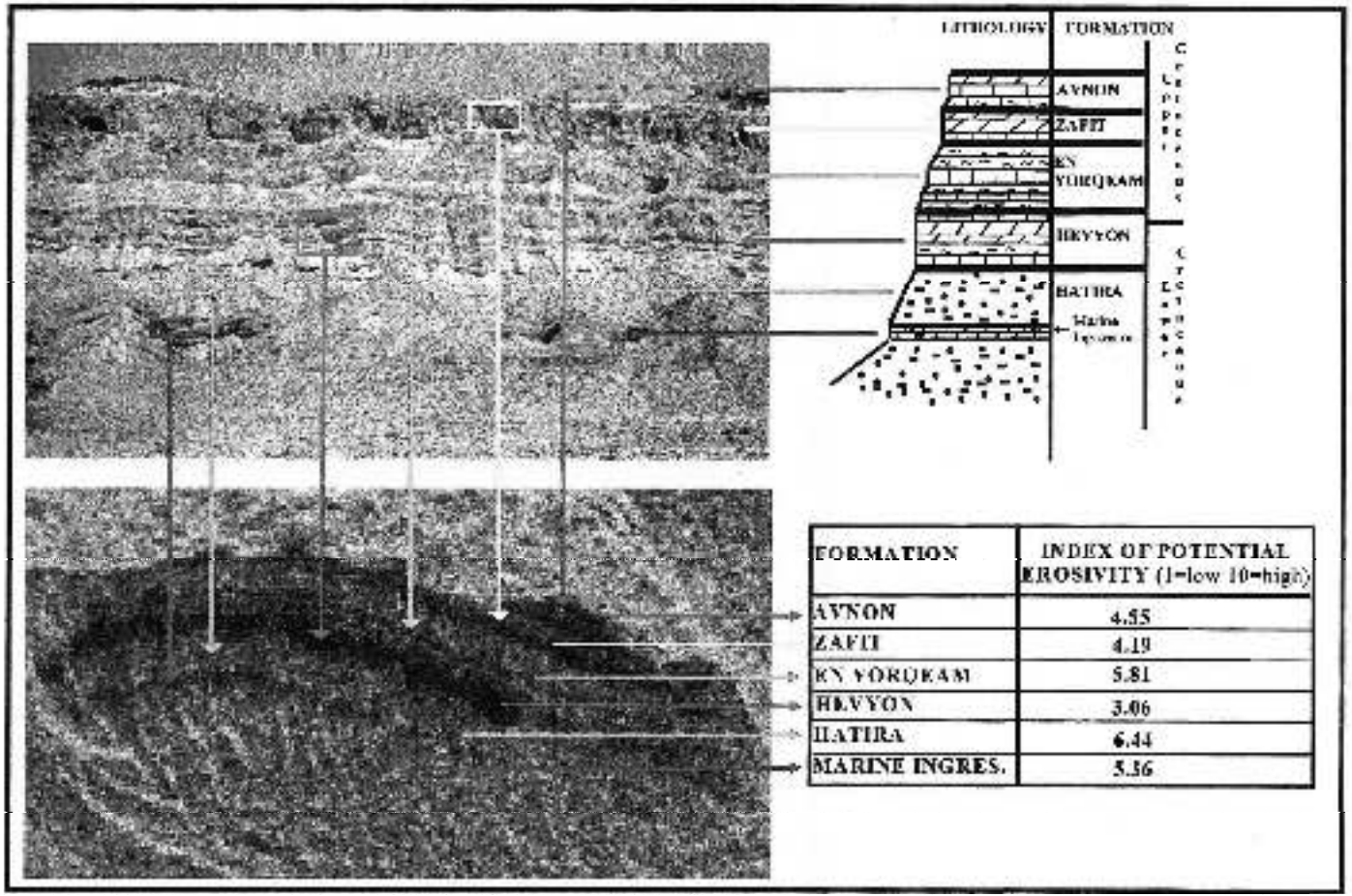

Figure 7. Summary of study. Identification of lithostratigraphy on geological formations and radar image in order to derive an index of potential erosivity.

sub-formation level or those that are currently not identified on geologic maps. It may also be used to supplement geological exploration in inaccessible regions or those of limited fieldwork possibilities. Furthermore, this method may aid in recognizing PE as it relates to civil engineering and risk–hazard applications.

Currently, DEDs are limited in their representation of cliff walls and often miss the subtle changes in ground slope due to differential bedding. The method presented in this paper may ultimately be utilized to enhance and refine representation of these cliff walls in existing DEMs. This will be possible because the correlation of cliff stratigraphy in terrain-corrected radar images is refined to combine with existing DEMs. The cliff wall and the SAR satellite sensor both 'looked' westward. Sensors with a look direction to the east can compliment and reveal similar banding patterns along east-facing cliff walls, thus providing additional data.

Further research on this subject and its methodology are encouraged. Avenues for this research may include correlating slope and dip of individual formations and stratum to their backscatter values; incorporating the influence of surface roughness on backscatter along talus slopes and cliff faces; and investigating the influence of SAR platforms with varying incidence angles to shed further light on these forward-facing cliffs.

Acknowledgments

The ERS-1 SAR scene was provided by the European Space Agency in the frame of the AO2-F112 research project. The work was jointly sponsored by the Israeli Ministry of Science and Art (through the Israel Space Agency) and the French Space Agency (CNES). The authors are very grateful to Dr Charles Ichoku for his help. Dr J. K. Hall kindly provided the DTM.

References

Arkin, Y., and Braun, M., 1965, Stratigraphic Sections No. 2a: Type Sections of Upper Cretaceous Formations in the Northern Negev (Jerusalem: State of Israel, Geological Survey).

Berlin, G. L., Schaber, G. G., Kozak, R. C., and Chavez, P. Jr, 1982, Cliff- and slope-topography of part of the Grand Canyon, as characterized on a Seasat radar image. Remote Sensing of Environment, **12**, 81–85.

Hirsch, F., 1996, Geological Map of Israel, Sheet 19-II, Hamakhtesh Hakatan (Jerusalem: State of Israel, Geological Survey).

Orni, E., and Efrat, E., 1976, Geography of Israel (Jerusalem: Israel Universities Press).